

This document is the Accepted Manuscript version of a Published Work that appeared in final form in Environmental Science & Technology, copyright © 2025 American Chemical Society after peer review and technical editing by the publisher. To access the final edited and published work see <https://doi.org/10.1021/acs.est.4c12324>.

1 Enhanced Soil Emissions of Reactive Nitrogen Gases
2 by Fertilization and Their Impacts on Secondary Air
3 Pollution in Eastern China

4 Chuanhua Ren^{1,2}, Xin Huang^{2,3*}, Yanan Wang¹, Li Zhang⁴, Xueyu Zhou², Weihang
5 Sun¹, Haoran Zhang², Tengyu Liu^{2,3}, Aijun Ding^{2,3}, Tao Wang^{1*}

6 ¹Department of Civil and Environmental Engineering, Hong Kong Polytechnic University, Hong
7 Kong 99907, China;

8 ²Joint International Research Laboratory of Atmospheric and Earth System Sciences, School of
9 Atmospheric Sciences, Nanjing University, Nanjing 210023, China;

10 ³Jiangsu Provincial Collaborative Innovation Center for Climate Change, Nanjing 210023, China;

11 ⁴California Air Resources Board, Riverside, CA 92507, USA

12 * Corresponding author: Xin Huang (xinhuang@nju.edu.cn), Tao Wang (tao.wang@polyu.edu.hk)

13 **KEYWORDS.** Fertilization, irrigation, soil nitrogen emissions, model simulation, air pollution.

14

15 **ABSTRACT.** Nitrogen fertilizer application is accompanied by intense release of multiple reactive
16 nitrogen (Nr) gases like nitrous acid (HONO), ammonia (NH₃), and nitric oxide (NO) from the soil,

17 influencing atmospheric chemistry and air pollution. In current emission inventories, post-
18 fertilization soil emissions are poorly characterized due to inaccurate identification of fertilization
19 timing and location. Moreover, pre-existing studies predominantly focus on individual Nr gases, and
20 a comprehensive understanding of simultaneously emitted Nr gases from fertilization and their
21 impacts on air quality is still limited. Here, we developed a novel method to identify the dryland
22 fertilization activity based on satellite and reanalysis datasets. Then, we updated a dynamic soil Nr
23 emissions model (WRF-SoilN-Chem) with lab-derived parameterization and applied it to analyze
24 the time- and space-varying Nr emissions and their effects on air quality. It is estimated that the Nr
25 emissions from a typical fertilization event in the Yangtze River Delta (YRD) region increased
26 ozone (O₃) and nitrate concentrations by 2.5% and 18.2%, respectively. HONO and NH₃ emissions
27 jointly enhanced nitrate via chemical production and gas-particle partitioning. An accurate
28 representation of fertilization and meteorology-emission-chemistry coupled modeling would greatly
29 improve the understanding of the soil Nr emissions and their impacts on regional air pollution.

30 **SYNOPSIS**

31 Our research reveals that the surging emissions of reactive nitrogen after fertilization exacerbate
32 air pollution by contributing to O₃ and PM_{2.5} formation.

33 **1. INTRODUCTION**

34 Agricultural soil emissions are important sources of atmospheric reactive nitrogen (Nr) gases¹⁻³,
35 including ammonia (NH₃), nitrous acid (HONO) and nitric oxide (NO), which are produced through
36 various microbial and chemical processes. Nitrogen fertilizer input significantly enhances Nr gases
37 emissions by increasing soil nitrogen content for microbial activities⁴⁻⁶. Field measurements and lab

38 experiments⁷⁻⁹ show that the Nr gases emissions peak 2–4 days later after fertilization with levels
39 5–100 times higher than in non-fertilization situations. Such intense Nr emissions, especially NH₃,
40 HONO and NO, collectively worsen air quality by contributing to the formation of tropospheric
41 ozone (O₃) and particulate matter (PM) via different chemical pathways¹⁰⁻¹⁶.

42 A variety of soil Nr emissions models¹⁷⁻¹⁹, including WRF-CMAQ-EPIC²⁰ (NH₃), WRF-SoilN-
43 Chem²¹ (NH₃), Yienger and Levy (YL)²² (NO), Model of Emissions of Gases and Aerosols from
44 Nature (MEGAN)²³ (NO) and Berkley-Dalhousie Iowa Soil NO Parameterization (BDISNP)²⁴ (NO)
45 have been developed and applied to investigate the role of soil Nr emissions on air quality. Sha et
46 al.²⁵ reveal the impacts of soil NO emissions on O₃ in rural California with the BDISNP model.
47 Wang et al.²⁶ demonstrate that soil HONO emissions aggravate O₃ and nitrate pollution in northern
48 China by WRF-CMAQ coupled with HONO parameterization. Pleim et al.²⁰ evaluate the NH₃
49 emitted from fertilized croplands and grasslands in North America with the WRF-CMAQ-EPIC
50 model. These models are effective in the assessment of individual Nr gases species. However, in
51 real agricultural fields, multiple gases are released concurrently after fertilization. A recent study
52 assesses the impact of soil HONO and NO emissions on O₃ and nitrate in a non-fertilization month²⁷.
53 So far, there has been little discussion on the simultaneous Nr gases emissions from fertilization and
54 their collective impacts on air quality.

55 Another challenge in fertilization relevant studies arises from the coarse or inaccurate fertilization
56 spatiotemporal information, which is attributable to the irregularity of farmlands and diverse
57 cultivation practices of smallholder farmers in China^{28,29}. As Nr surging emissions appear 2–4 days
58 after fertilization, exact dates and location of fertilization are critical for soil emissions analysis. The
59 pre-existing studies typically obtain fertilization information from crop calendars or surveys of local
60 farmers³⁰⁻³². However, crop calendars with a temporal resolution of 1–2 months are insufficiently

61 detailed to accurately capture surging soil emissions lasting only 1–2 weeks. Furthermore, the
62 questionnaire method is labor-intensive and time-consuming, particularly in large agricultural
63 regions like the North China Plain (NCP) and the Yangtze River Delta (YRD).

64 In this work, we aim to clarify the impact of fertilization Nr emissions on regional air quality using
65 a novel approach to identify daily dryland fertilization and an updated emissions model
66 incorporating dynamic soil NO, HONO and NH₃ parameterization. We chose the YRD, which has
67 extensive and fertile croplands, as a case study region to apply this new approach and model for
68 analysis. The results indicate that the intense Nr emissions during a typical fertilization activity
69 noticeably enhance ambient oxidizing capacity and promote nitrate formation. This work advances
70 understanding of the effects of fertilization-induced Nr emissions on air pollution, emphasizing the
71 need for considering agricultural emissions in future air quality strategies.

72 **MATERIALS AND METHODS**

73 **2.1 Identification method of fertilization events**

74 In light of the limitation concerning fertilization spatiotemporal information, we propose a novel
75 method for identifying fertilization events in drylands based on multiple datasets, including the crop
76 calendar, land use, satellite soil moisture measurements, and reanalysis data of soil moisture. This
77 methodology is mainly based on two key features in crop cultivation practices.

78 Firstly, fertilization and irrigation are typically carried out concurrently during the sowing season.
79 In modern cultivation practices, farmers usually drill the fertilizer together with seed to optimize
80 labor efficiency and subsequently irrigate the fertilized soil immediately (within approximately 30
81 mins)^{33,34} to facilitate the fertilizer hydrolysis and maintain soil moisture for seed germination³⁵. In
82 regions with higher mechanization level like the NCP or YRD, farmers adopt the Water-Fertilization

83 Integration (WFI) technique that mixes fertilizer with water and delivers the mixture to soil through
84 a pipe or pressure system to supply nutrients directly to the crop³⁶. Such synchrony between the two
85 processes makes it reasonable to identify fertilization events through irrigation occurrence.

86 Secondly, the disparity of soil moisture dry-wet transition trends between satellite and reanalysis
87 data can serve as an indicator of irrigation activities. Satellite directly detect soil brightness
88 temperature and calculate soil moisture^{37,38}. Thus, both natural rainfall and irrigation-induced soil
89 wetting can be detected by the satellite measurements³⁹. However, unlike direct measurements by
90 satellite, reanalysis data is generated by combining historical observations with model outputs using
91 data assimilation techniques. This process assimilates precipitation but does not incorporate human
92 activities like irrigation; hence, reanalysis data cannot represent irrigation-induced soil wetting^{40,41}.
93 Therefore, a daily comparison between satellite observations and reanalysis data on different areas
94 can identify the timing and location of irrigation. The concurrency of fertilization and irrigation
95 makes it possible to derive the spatiotemporal distribution of fertilization with a spatial resolution
96 of 25 km, following the soil moisture data resolution.

97 This identification method is suitable for most dryland crops but has limitations on wetland crops
98 such as rice, taro and other semi-aquatic crops, where the reliability of the satellite retrievals is far
99 lower than those in drylands⁴². Though this method is applicable to basal fertilization during the
100 planting season, it may not be feasible during the growing season when irrigation and fertilization
101 can be conducted separately. As dryland constitutes the majority of China's cropland (i.e., 75.45%)⁴³,
102 and the basal fertilization accounts for 63% of the total fertilizer consumption for dryland crops⁴⁴,
103 this method is thus applicable under most cultivation situations in China.

104 **2.2 Implementation of soil HONO and NO emissions in WRF-SoilN-Chem**

105 WRF-SoilN-Chem is a dynamic soil Nr emissions model coupled with meteorology–chemistry
 106 transport model WRF-Chem, capable of numerically describing agriculture Nr emissions rate
 107 interactively with time- and spatial-varying meteorological and soil conditions. In the original
 108 version WRF-SoilN-Chem, dynamic fertilization NH₃ emission flux is obtained by multiplying
 109 static basic emissions (Basic E_{NH₃}) with dynamic emission correction factors (CF), as shown in Eq
 110 (1) and Eq (2). The descriptions of the model parameterization and evaluation are detailed in Ren et
 111 al.²¹

$$112$$

$$113 \quad Flux_{NH_3-fertilizer} = Basic E(NH_3)_{fertilizer} \times CF_{wind} \times CF_{soil_T} \times CF_{soil_m} \times CF_{rain} \quad (1)$$

$$114 \quad EF_{static_{fertilizer}} = EF_{0i} \times CF_{pH} \times CF_{method} \times CF_{rate} \times CF_{time} \quad (2)$$

115 Where $Flux_{NH_3-fertilizer}$ (mol km⁻² h⁻¹) is the dynamic NH₃ emission flux from fertilization.
 116 $Basic E(NH_3)_{fertilizer}$ (mol km⁻² h⁻¹) is the basic NH₃ emission flux from fertilization, which is
 117 calculated from nitrogen fertilizer rate multiply by static emission factor ($EF_{static_{fertilizer}}$) at a
 118 specific condition. CF_{wind} , CF_{soil_T} , CF_{soil_m} and CF_{rain} are the dynamic meteorological correction
 119 factors (CF) for wind speed, soil temperature, soil moisture content and rainfall, respectively. EF_{0i}
 120 is the reference emission factor for different nitrogen fertilizers. CF_{pH} is the correction factor for
 121 different soil acidity; CF_{method} is for fertilization application method, including basal dressing and
 122 top dressing; CF_{rate} is for different application rates, and CF_{time} is for time since fertilizer application,
 123 which is used to reflect the variation characters of NH₃ emission after fertilization. The detailed
 124 parameterizations of these CF are described in the Table S1.

125 In this work, we updated the model by incorporating additional soil HONO and NO emissions
 126 based on Oswald et al.,⁴⁵ Zhang et al.⁴⁶ and Wang et al.²⁶ Given the substantial differences in Nr
 127 gases emissions before and after fertilization, we classified agricultural soil emissions into two states:

128 the post-fertilization state and the background state. Since Nr emissions usually peak 2–4 days after
 129 fertilization and return to non-fertilization level within 10 days, the post-fertilization state is defined
 130 as “within 10 days after fertilizer application”. The background state is defined as “before
 131 fertilization” or “10 days later after fertilization” time, when Nr emissions are at a low level.

132 For HONO emission in the background state, Oswald et al.⁴⁵ estimated HONO optimum emission
 133 ($F_{N, opt}$) from different soil samples like forest, pasture, grassland, wheat and cotton fields. The
 134 optimum soil HONO flux is scaled by the function of soil temperature (T) and soil water content
 135 (SWC), based on laboratory experiments, the parameterization is Eq (3):

$$136 \quad F_{SHONO} = F_{N, opt} \times h(T) \times g(SWC) \quad (3)$$

137 where $F_{N, opt}$ is the optimum flux of HONO in terms of N mass ($\text{ng N m}^{-2} \text{s}^{-1}$). $h(T)$ is a dimensionless
 138 function of HONO emissions with respect to soil T, and $g(SWC)$ is the function of HONO emissions
 139 on SWC (% water-holding capacity (WHC)).

140 For HONO emissions in the post-fertilization state, we utilized the fertilization parameterization
 141 of Wang et al.²⁶ to represent the enhanced HONO emissions after fertilization within 10 days. The
 142 post-fertilization HONO emissions (F_{SHONO}) are predicted as a function of soil temperature and
 143 SWC in Eq (4). The detailed equation method and parameters can be found in Wang et al.:²⁶

$$144 \quad F_{SHONO} = F_{emis(HONO)}(Dry\ peak) + F_{emis(HONO)}(wet\ peak) = [F_{N, maxDry} \cdot \exp\left(-\frac{(SWC - SWC_{CDry})^2}{w_{Dry}^2}\right) +$$

$$145 \quad F_{N, maxWet} \cdot \exp\left(-\frac{(SWC - SWC_{CWet})^2}{w_{Wet}^2}\right)] \times \exp\left[\left(-\frac{43900}{R}\right) \cdot \left(\frac{1}{T} - \frac{1}{298}\right)\right]$$

146 (4)

147 $F_{emis}(Dry\ peak)$ is the fitted Gaussian function in the low SWC range (0-60% WHC) and
 148 $F_{emis}(wet\ peak)$ is in the high SWC range (60-100% WHC), $F_{N, max}$ is the maximum HONO flux
 149 at the optimum SWC ($SWC_{Cwet/dry}$) at the reference temperature 298 K, w characterizes the width of

150 the curves. The *dry* and *wet* subscripts represent the parameters on dry peak and wet peak,
 151 respectively. R is the gas constant ($8.314 \text{ J mol}^{-1} \text{ K}^{-1}$).

152 Given that the default WRF-Chem model includes only one pathway for HONO formation via
 153 hydroxyl radical (OH) and NO, we integrated additional sources, including vehicle emissions and
 154 secondary pathways (Table S2, S3), to enhance the accuracy of HONO concentration estimation and
 155 assess the contributions of post-fertilization to HONO.

156 For NO, the background and post-fertilization soil NO emission schemes are from Wang et al.²⁷
 157 and Wang et al.²⁶ respectively. In these schemes, the NO flux is calculated based on the maximum
 158 NO flux under optimum condition ($F_{N,max}(\text{NO})$), and further adjusted by soil water content and soil
 159 temperature, similar to the approach used for HONO. The NO parameterization equation (Eq (5))
 160 follows the same form as the HONO equation. The difference lies in the value of parameters like
 161 $F_{N,maxDry}$, $F_{N,maxWet}$, $SWC_{C_{Wet}}$, $SWC_{C_{Dry}}$, w_{Wet} , and w_{Dry} , which are derived from the curve
 162 fitting of HONO and NO flux data. The specific values of these parameters are provided in Table
 163 S4.

$$\begin{aligned}
 164 \quad F_{NO} = F_{emis(NO)}(Dry\ peak) + F_{emis(NO)}(wet\ peak) = [F_{N,maxDry} \cdot \exp\left(-\frac{(SWC-SWC_{C_{Dry}})^2}{w_{Dry}^2}\right) + F_{N,maxWet} \cdot \\
 165 \quad \exp\left(-\frac{(SWC-SWC_{C_{Wet}})^2}{w_{Wet}^2}\right)] \times \exp\left[\left(-\frac{43900}{R}\right) \cdot \left(\frac{1}{T} - \frac{1}{298}\right)\right] \quad (5)
 \end{aligned}$$

166 Since the measured HONO and NO emissions may include contributions from each other due to
 167 the oxidation of NO to HONO, as well as the rapid photolysis of HONO to NO, Wang et al.²⁶ placed
 168 the entire sampling setup inside dark cabinet and dried the soil with purified air throughout the
 169 experiment to minimize the transformation between HONO and NO and obtain more accurate
 170 measurements. Given the diagnosed model includes individual chemical reaction processes, such

171 explicit HONO and NO soil emissions in the atmospheric chemistry model are essential for
172 providing detailed diagnosis and quantification of the impacts on air quality.

173 **2.3 Model configuration and simulation design**

174 To evaluate the model performance of the updated WRF-SoilN-Chem and the air quality response
175 to soil Nr emissions, we designed six parallel experiments: Base, HONO, NH₃, NO, NH₃+HONO,
176 NH₃+HONO+NO. The Base experiment applied the anthropogenic emission inventory for 2020
177 from the Multi-resolution Emission Inventory for China (MEIC)^{47,48} but excluded the fertilization
178 and soil emissions of all Nr gases. Other sensitivity experiments were conducted by introducing
179 additional soil Nr emissions into Base experiment, as detailed in Table 1. We adopt fertilizer
180 application of 100 kg N ha⁻¹ during the identified basal fertilization stage, following the fertilization
181 rate statistics in the YRD provided by Zhang et al.⁴⁹ To investigate fertilization Nr emission and its
182 impact on air quality during the whole time period of the identified fertilization event (see Results
183 3.2), simulations are conducted from 20 Sep to 10 Oct 2021, with first 10 days as a spin-up time.
184 The model domain covers eastern China (18° N–50° N, 95° E–131° E) with a 20 km grid resolution.
185 Other key settings are detailed in Text S1 and Table S5. The simulations of key surface
186 meteorological parameters and pollutants are validated by available observations in Figure S1–S3.
187 The normalized mean biases of temperatures, RH and wind speed in Nanjing are –3.6%, 1.7%, and
188 35.9%, respectively. The simulation well captures the spatial pattern and pollution level of PM_{2.5},
189 CO, O₃, NO₂, nitrate and ammonium concentrations measured by surface stations in the YRD
190 (Figure S2–S3).

191 As mentioned in Section 2.1, reanalysis data could not accurately simulate irrigation-induced soil
192 wetting. Since soil moisture directly affects soil emissions simulation, we used satellite-detected

193 moisture to drive the simulation. Based on the method from Jared et al.,⁵⁰ we assimilated the satellite
 194 soil moisture retrievals at 00 UTC in all experiments.

195 **Table 1. Simulation experiment design considering different sources of soil Nr emissions**
 196

Experiments	Additional fertilization emissions considered		
	Soil HONO	Soil NH ₃	Soil NO
Base	×	×	×
HONO	✓	×	×
NH ₃	×	✓	×
NO	×	×	✓
NH ₃ +HONO	✓	✓	×
NH ₃ +HONO+NO	✓	✓	✓

197

198 **2.4 Identification of potential air mass source regions**

199 The Lagrangian particle dispersion modeling (LPDM) was conducted using the Hybrid Single-
 200 Particle Lagrangian Integrated Trajectory model (HYSPLIT) driven by Global Data Assimilation
 201 System (GDAS) to identify the potential sources of air masses during the studied pollution case⁵¹.
 202 The LPDM was run in the 24-hour backward mode, with 3,000 particles released every 2 hours over
 203 the Nanjing station. Particle residence times below 100 m were used to identify the “footprint” of
 204 air masses arriving at the Nanjing station. The spatiotemporal distributions of these particles were
 205 used to identify potential source regions and their relative contributions to air masses at Nanjing
 206 station.

207 **2.5 Datasets**

208 **2.5.1 In situ measurements**

209 Hourly concentrations of NH₃, HONO, O₃, nitrogen dioxide (NO₂), carbon monoxide (CO), sulfur
 210 dioxide (SO₂), and PM_{2.5} were measured at the Station for Observing Regional Processes of the
 211 Earth System (SORPES, 32°07'14' N, 118°57'10' E; ~40 m a.s.l.) in Nanjing, Jiangsu province.
 212 NH₃ concentrations were measured with a Picarro G2103 gas analyzer (Picarro Inc., USA) that

213 employs cavity ring-down spectroscopy (CRDS) technique⁵². HONO concentrations were measured
214 using a commercial long-path absorption photometer instrument (LOPAP)⁵³. NO_x, O₃, and CO were
215 measured by Thermo Fisher analyzers (TEI 42i, 49i, and 48i, USA, respectively). The PM_{2.5}
216 concentrations were detected using a mass analyzer (Thermo SHARP-5030). Furthermore, aerosol
217 components, including sulfate (SO₄²⁻), nitrate (NO₃⁻) and ammonium (NH₄⁺) were measured by a
218 Monitor for Aerosols and Gases in ambient Air (MARGA).

219 In addition to the data from SORPES, hourly PM_{2.5}, SO₂, NO₂, O₃, and CO data from other YRD
220 cities were obtained from China's Air Quality Monitoring Network⁵⁴. The meteorological
221 observations, including wind, temperature, precipitation and relative humidity, were obtained from
222 the National Climatic Data Center's (NCDC) Integrated Surface Database (ISD).

223 **2.5.2 Soil moisture datasets**

224 Soil moisture observations from the satellite were obtained using the Advanced Microwave
225 Scanning Radiometer–Earth Observing System and version 2 (AMSR–E/AMSR2) instruments.
226 Previous assessments have shown that the AMSR instruments are highly sensitive to changes in soil
227 moisture, whether they're caused by rainfall or irrigation³⁹. This sensitivity is reflected in the strong
228 correlation between satellite and aircraft soil moisture measurements, both spatially (average R =
229 0.92 and RMSD = 0.049 m³ m⁻³) and over time (R = 0.94 and RMSD = 0.04 m³ m⁻³)⁵⁵. The data
230 provided by this product covers a 25×25 km² area and is updated daily, making it a valuable resource
231 for monitoring soil conditions.

232 The hourly soil moisture reanalysis data used in this study is from ECMWF Reanalysis v5 (ERA5)
233 ⁵⁶. ERA5 assimilates precipitation data from the Tropical Rainfall Measuring Mission Microwave
234 Imager (TRMM–MI), and demonstrated outstanding soil moisture dynamic properties in past
235 evaluations⁵⁷.

236 2.5.3 Crop planting datasets

237 The planting day of crops in YRD region is obtained from the Global Gridded Crop Model
238 Intercomparison (GGCMI) Phase 3 dataset⁵⁸. It provides in each 0.5° land grid cell the planting day
239 and maturity day for 18 different crops, separating rainfed and irrigated systems. To represent the
240 crop planting intensity in different seasons, we calculate the crop planting ratio in each month as
241 follows:

$$242 \text{ Planting ratio}_{(m)}(\%) = \frac{F_{(m)}}{\sum_{m=1}^{12} F_{(m)}} = \frac{\sum_i \sum_j \sum_c N_{(c,i,j,m)}}{\sum_m \sum_i \sum_j \sum_c N_{(c,i,j,m)}} \quad (6)$$

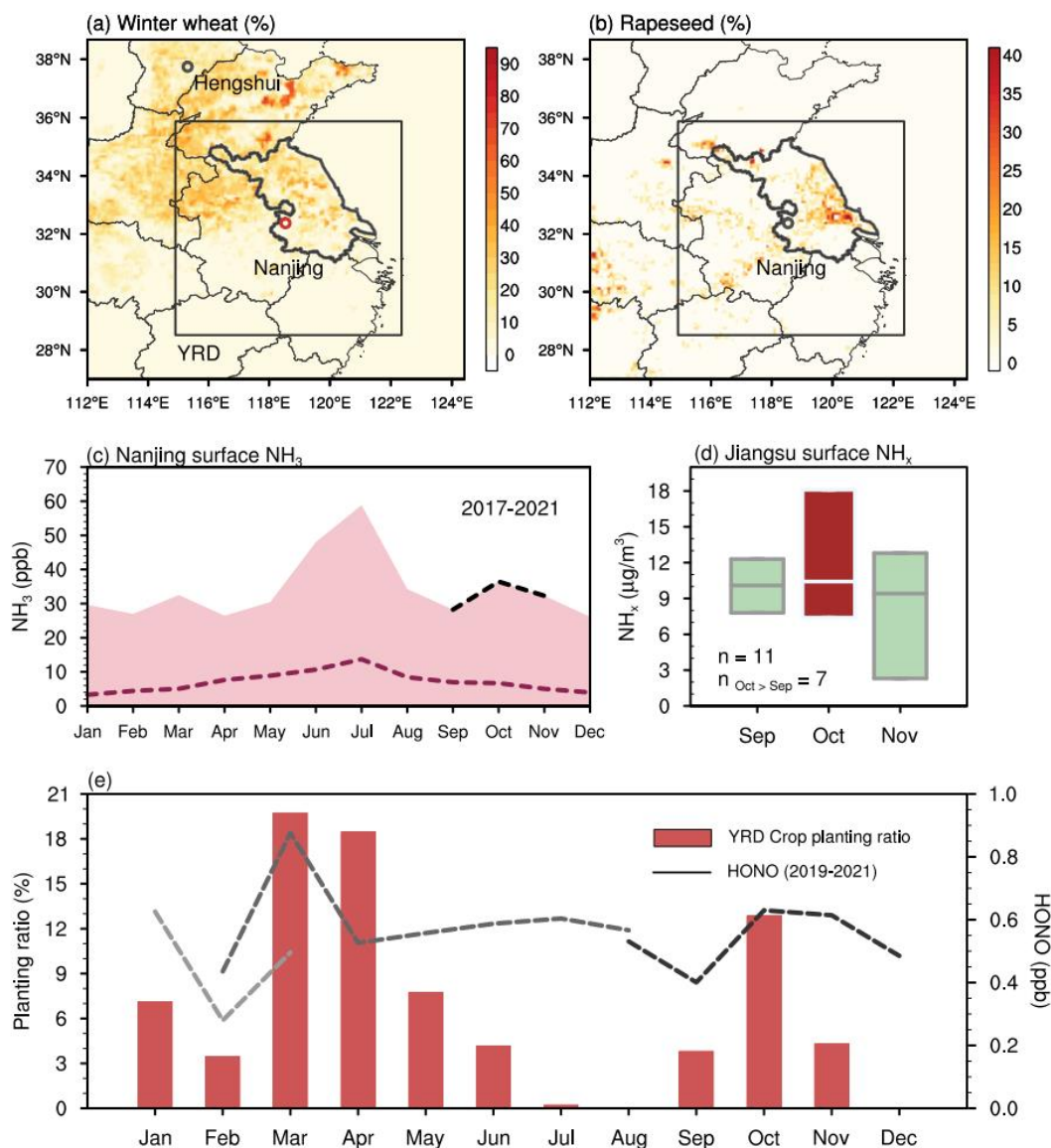
243 where c represents the crop type, m denotes the month in a year, and i and j are the location indices
244 of the data grid. N indicates the planting event, where $N=1$ means a planting event occurs, and $N=0$
245 otherwise. $F_{(m)}$ is the frequency of planting events in each month, calculated by summing up the
246 planting events for each crop type, each grid, and each day within the month.

247 3. RESULTS AND DISCUSSION

248 3.1 Enhanced HONO and NH₃ concentration during the fertilization period

249 The YRD region, covering approximately 126,505 km² of cultivated land (9.3% of the national
250 cultivated land area), features the most fertile soil in China⁵⁹ and is highly suitable conditions for
251 crop farming. Rice, wheat and rapeseed are the main economic crops grown in the YRD region⁶⁰.
252 Rice is the staple crop distributed across most areas of the YRD region, whereas winter wheat and
253 rapeseed are mainly cultivated in northern (Figure 1a) and eastern Jiangsu province (Figure 1b),
254 respectively. According to the crop calendar, early rice and spring corn are sown from March to
255 April, and winter wheat and rapeseed are predominantly planted in October. Therefore, the crop
256 planting seasons in the YRD are mainly concentrated in March, April and October (Figure 1e).

257 Intensive agricultural crop cultivation makes the YRD a hot spot region for agricultural Nr gases
258 emissions⁶¹. Persistently extensive planting activities accompanied with fertilization lead to
259 substantial locally emitted Nr pollutants, and thus ambient Nr concentrations and crop planting ratio
260 exhibit similar peaking time in the planting season. Multiyear observations (2017–2021) from
261 Nanjing SORPES station showed that the average HONO, the maximum NH₃ concentration and the
262 crop planting ratio peaked in January, March and October (Figure 1c, 1e). The Pearson correlation
263 coefficient between Nr concentrations and planting ratio is 0.58. Besides Nanjing, other rural sites
264 (for example, Fengyang in Anhui province and Fenghua in Zhejiang province) in the YRD exhibited
265 a similar phenomenon of higher Nr concentrations in the sowing season (Figure 1d). As clearly
266 demonstrated in Figure 1d and Figure S4, the substantial enhancement of both ground and satellite
267 observed NH₃ in October (the sowing month) than in September (the warmer month), indicates a
268 more important role of fertilization than warmer temperature in Nr emissions.



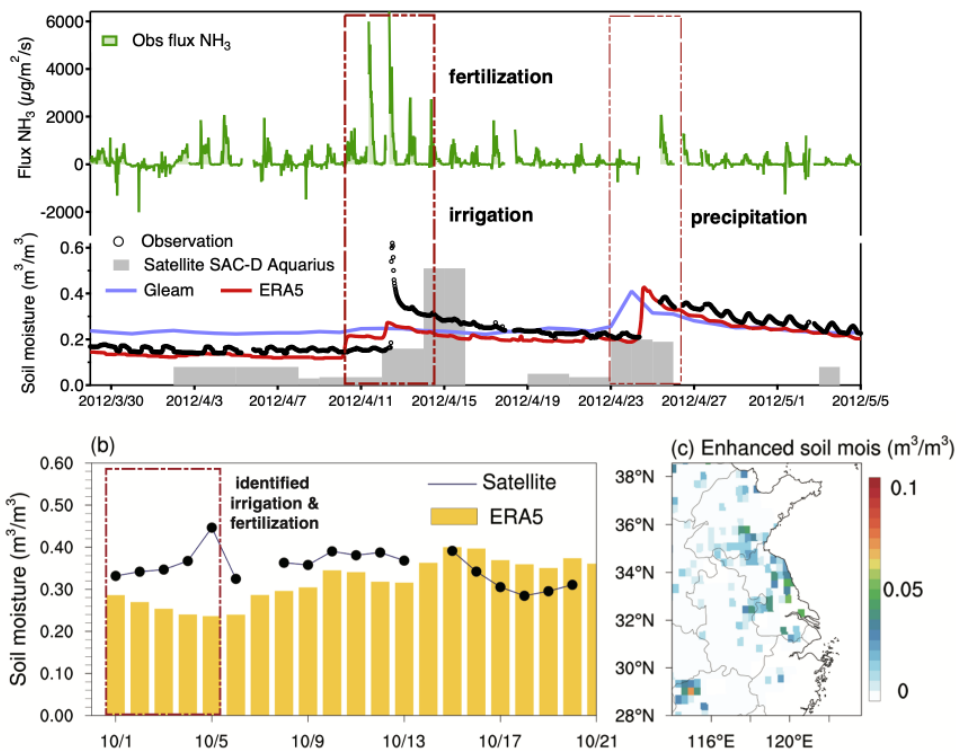
269
 270 Figure 1. Observational evidence of fertilization effects on Nr concentrations. Percentage of (a)
 271 winter wheat and (b) rapeseed coverage⁶² at 20 m resolution in the YRD region (black box), and the
 272 black thick line outlines the Jiangsu province. (c) Averaged NH_3 concentration in Nanjing SORPES
 273 site during 2017–2021, the upper and lower edge of the filled area is 99% and 1%. (d) The mean
 274 surface NH_x ($\text{NH}_3(\text{gas}) + \text{NH}_4^+(\text{aerosol})$) concentration of the YRD region sites from 2011–2015
 275 according to the nationwide nitrogen deposition monitoring network (NNDMN) dataset⁶³, n is the
 276 count of valid value. (e) The YRD seasonal crop planting ratio and HONO concentration in Nanjing.

277 **3.2 Post-fertilization soil Nr emissions and their regional transport**

278 By evaluating the method in Section 2.1 and applying it to identify a typical fertilization event in
279 the YRD, we can investigate the post-fertilization effects on air quality. Previous field measurements
280 of post-fertilization fluxes in the YRD region have supported our identification method with
281 observations of the simultaneous increase in Nr emissions and soil moisture following fertilization
282 and irrigation during the sowing period^{64,65}. The high-resolution field measurements conducted by
283 our research group in a crop field in Hengshui city (Hebei province of China) provides another
284 opportunity to verify our identification method. As shown in Fig. 2a, during the corn planting season
285 (April 2012), as farmers applied fertilizer and irrigated the soil, both the NH₃ emission flux and soil
286 moisture simultaneously increased by 4–6 times on April 12th. The soil moisture from satellite
287 observations and reanalysis data showed different dry-wet transitions by the irrigation. Specifically,
288 the soil moisture from the SAC-D (Satélite de Aplicaciones Científicas) satellite effectively captures
289 the dry-wet transition caused by irrigation and rainfall events on April 12th and April 24th,
290 respectively. However, the Global Land Evaporation Amsterdam Model (GLEAM) and ERA5,
291 which only assimilate precipitation, only indicate soil moisture increase due to rainfall on April 24th.
292 In short, the combination of the satellite and reanalysis data is able to distinguish the fertilization
293 event.

294 Considering the noisy performance of satellite data on waterlogged paddy fields, we examined the
295 bare drylands sown with wheat and rapeseed in October in the YRD region. Figure 2b shows
296 different temporal trends between ERA5 reanalysis and the AMSR satellite datasets in early October.
297 The satellite-observed soil moisture increased continuously from October 1st to 5th, while the ERA5
298 value remained stable. The Integrated Multi-satellitE Retrievals for Global Precipitation
299 Measurement (IMERG) (Figure S5) shows no precipitation during this period, suggesting that the

300 soil wetting was dominantly caused by irrigation. As displayed in Figure 2c, the soil wetting was
 301 most pronounced in eastern and northern Jiangsu province, overlapping with the wheat and rapeseed
 302 cultivation areas, further confirming the occurrence of irrigation and fertilization. Besides this
 303 observational evidence, the official guidelines from the Ministry of Agriculture and Rural Affairs
 304 recommend early October (Oct 1st–10th) as the optimum time for sowing and fertilizing winter wheat
 305 and rapeseed in the “Huaihe River Basin” and “Yangtze-Huaihe region”⁶⁶ in 2021. The above
 306 analyses confirm the occurrence of fertilizer application from October 1st to 5th, and support the
 307 feasibility of the proposed method for determining the timing and location of fertilization.
 308



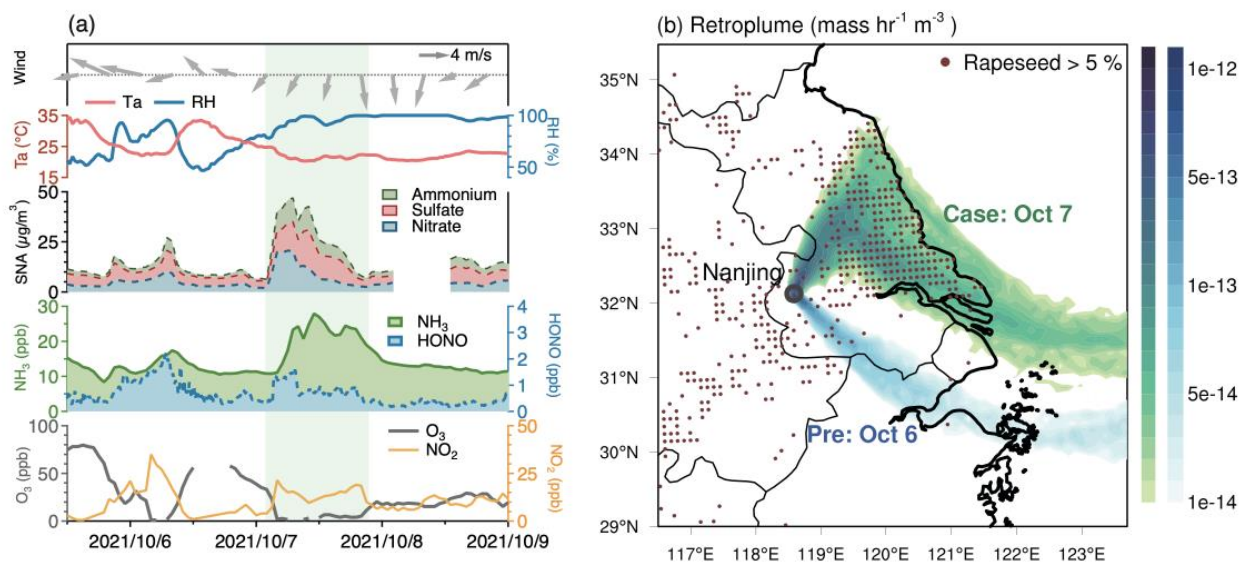
309
 310 Figure 2. Identification of the timing and location of a fertilization and irrigation event. (a) Time
 311 series of the observed ammonia flux and moisture in Hengshui farmland, Hebei province of China.
 312 The grey bar refers to the soil moisture from satellite SAC-D Aquarius, and the purple and red lines

313 are the GLEAM and ERA5 reanalysis datasets, respectively. The black circle markers indicate the
314 field measurements. (b) Daily satellite-detected and ERA5 soil moisture on Jiangsu croplands in
315 October 2021, and the bounding red box represents the identified irrigation and fertilization dates.
316 (c) The enhanced soil moisture from Oct 1st to Oct 5th 2021.

317 An air pollution episode occurring 2 days after the extensive fertilization showed a plausible
318 connection with fertilization-related nitrogen emissions. As shown in Fig. 3a, on the morning of Oct
319 7th, high levels of HONO, NH₃, sulfate, nitrate and ammonium (SNA) with the prevailing northerly
320 wind were recorded in Nanjing SORPES station. The pollution episode lasted for 1 day with
321 maximum NH₃ reaching up to 30 ppb, which was 5 times higher than clean state. The satellite
322 retrieval also demonstrated the NH₃ hotspot in Jiangsu province on Oct 7th (Figure S6). As
323 agricultural activity is the major source of NH₃, the sudden rise in pollutant concentrations
324 accompanied by changing wind direction indicated that both agricultural emissions and regional
325 transport are probable causes of this pollution event.

326 The Goddard Earth Observing System (GEOS) model with assimilation showed that the nitrate
327 and sulfate pollution was partly transported from North and South Korea to Nanjing along with the
328 northerly wind (Figure S7). The base experiment without post-fertilization was able to reproduce
329 the rise of nitrate concentration caused by such regional transport, but still obviously underestimated
330 it (Figure S8), indicating the missing of potential source. Source attribution based on LPDM showed
331 that the air mass on the polluted (Oct 7th) day originated from the ocean and passed through the
332 extensively fertilized rapeseed plots (Figure 3b). Along the transport pathway, the upstream soil-
333 emitted Nr gases were carried to Nanjing, contributing to the observed increase in fine particle
334 pollution, particularly ammonia and associated secondary aerosols.

335 The lifetime of ammonia is approximately 12 hours⁶⁷ and our calculations indicate that such
 336 lifetime is sufficient long for NH₃ emitted from the farthest Jiangsu fields to be transported to
 337 Nanjing. In comparison, noontime HONO is short-lived (10–20 mins) and originates from various
 338 sources, including traffic emissions and heterogeneous reactions. Due to its rapid photolysis, HONO
 339 emitted during the daytime from eastern Jiangsu is unlikely to reach Nanjing SORPES via long-
 340 range transport. Only emissions from nearby farmlands can contribute to HONO levels observed at
 341 SORPES station. However, the HONO emitted from distant farmlands can contribute to the
 342 formation of longer-lived pollutants such as O₃ or SNA, which exert broader and prolonged effects⁶⁸.
 343
 344



345
 346 Figure 3. A typical air pollution episode and the potential impact from agricultural sources. (a) Time
 347 series of meteorological parameters (air temperature (Ta), relative humidity (RH), wind), the
 348 concentrations of NH₃, HONO, O₃, NO₂, and ammonium, sulfate and nitrate at the SORPES station
 349 in Nanjing during October 5th–9th 2021. The pollution period is marked by the green box. (b) 24-

350 hour backward retroplume of Nanjing on clean day Oct 6th (blue) and polluted day Oct 7th (green).
351 The brown dots represent the agricultural fields with more than 5% rapeseed planting.

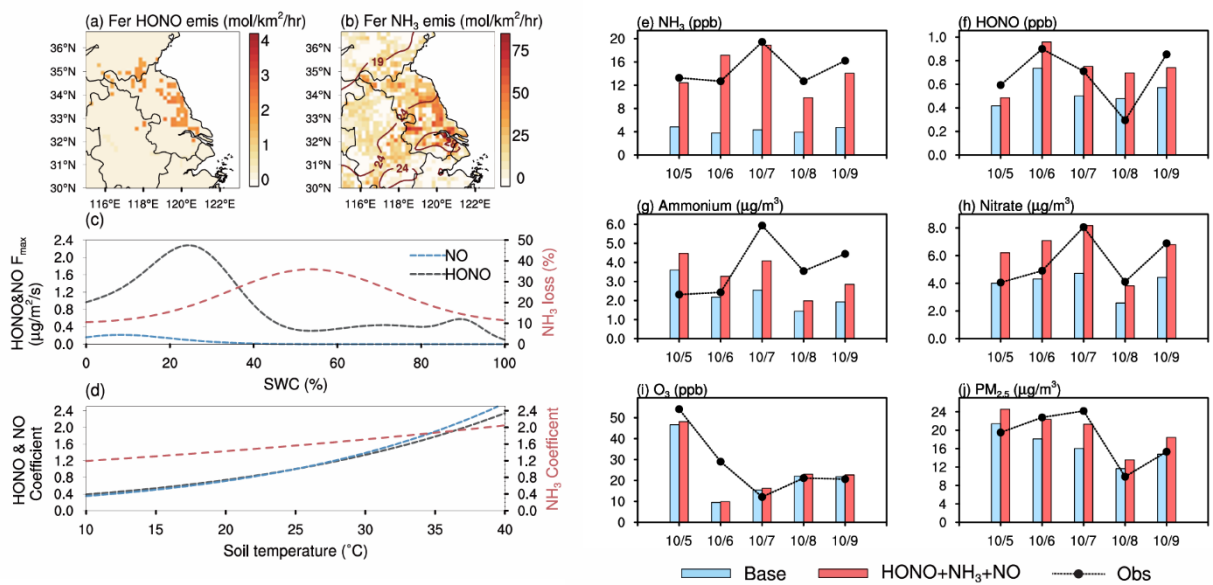
352 **3.3 Quantifying fertilized soil Nr emissions and their impacts on air pollution**

353 To investigate the impacts of fertilization emissions on air quality, we performed diagnosed
354 simulations with an air quality model incorporating with dynamic soil Nr emissions (WRF-SoilN-
355 Chem, see Methods). In the YRD region, the simulated emissions of NH₃ and HONO (Figure 4a,
356 4b) and NO (Figure S9) during the post-fertilization period (October 1st–10th) were 28.5, 1.09 and
357 0.19 mol km⁻² hr⁻¹, respectively, in good agreement with the Nr flux measured by Zhao et al.⁶⁹, Xia
358 et al.⁶⁴ and Wang et al.²⁷ in the YRD (Table S6). The spatial patterns of these Nr emissions show
359 notable heterogeneity across different species. For HONO and NO, emissions were concentrated in
360 eastern and northern Jiangsu, where soil moisture was elevated (~30% WHC) after irrigation (Figure
361 S10). For NH₃, high emissions are not only concentrated in eastern and northern Jiangsu but also in
362 the southern Jiangsu. This spatial heterogeneity can be attributed to their distinct sensitivities to soil
363 moisture and soil temperature. According to the Nr emission parameterizations, the NH₃ emission
364 peaks at 50% WHC⁷⁰, the HONO peaks at 25% and 90% WHC, and the NO at 10% WHC (Figure
365 4c). Thus, the irrigated soil moisture conditions (~30% WHC) are more favorable for peak HONO
366 emissions to occur. Under the same soil temperature, the NH₃ emission factor is larger than HONO
367 (Figure 4d)^{71,72}. During the case period, the soil temperature in the southern Jiangsu was 7–9 °C
368 higher than that in the northern part. Such high temperature led to a substantial increase in NH₃
369 emissions in the southern region, resulting in regional heterogeneity in Nr emissions.

370 The fertilization Nr emissions significantly improved the simulation of relevant pollutants in
371 Nanjing SORPES site during the pollution period (Figure 4e–j, Figure S11). Agricultural NH₃
372 emissions from upstream regions improved the simulation of NH₃ in Nanjing, both in magnitude

373 and temporal variation (Figure 4e). As an alkaline gas, NH_3 can react with ambient sulfuric acid
 374 (H_2SO_4) and nitric acid (HNO_3) to form $(\text{NH}_4)_2\text{SO}_4$, NH_4HSO_4 and NH_4NO_3 aerosols; hence, the
 375 enhanced NH_3 also mitigates the underestimation of NH_4^+ , NO_3^- , and $\text{PM}_{2.5}$ (Figure S12). The base
 376 experiment revealed a slight underestimation of HONO compared to NH_3 (Figure 4f), indicating
 377 that local non-agricultural sources dominate HONO production at SORPES (Figure S13a). Despite
 378 this, additional soil HONO emissions contributed to elevated the nitrate and $\text{PM}_{2.5}$ concentrations
 379 (Figure S12). In contrast, soil NO emissions were negligible relative to HONO and NH_3 , resulting in
 380 minimal effect on air quality in this case (Figure S14).

381



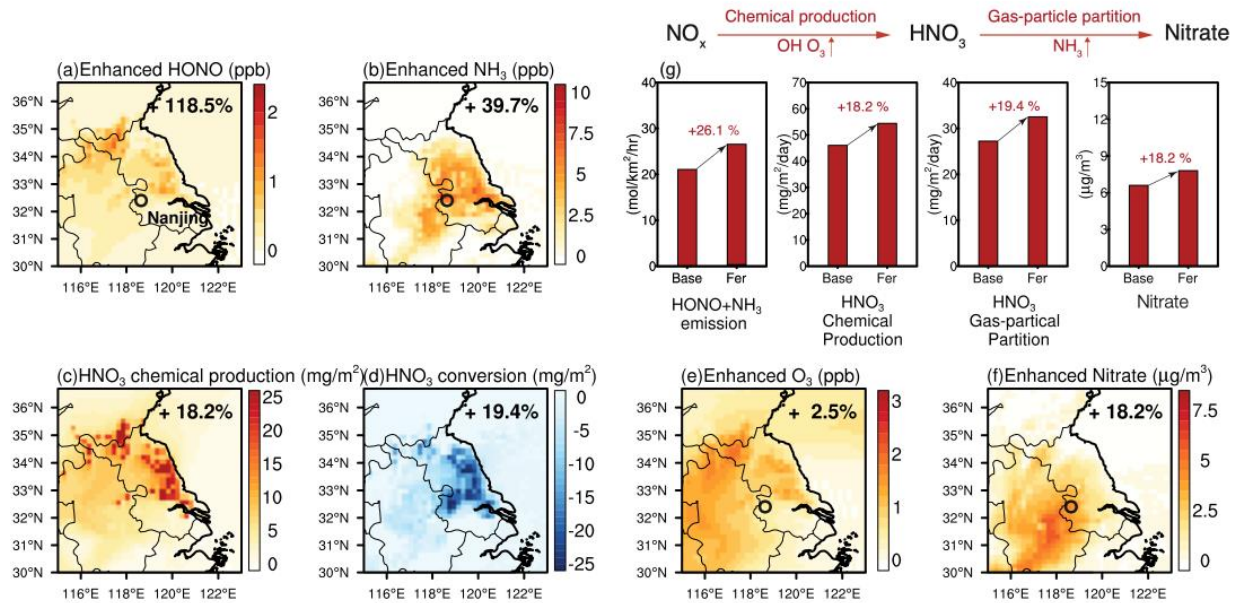
382

383 Figure 4. Improved model performance on air quality by including fertilization Nr emissions. Spatial
 384 distribution of simulated (a) HONO and (b) NH_3 fertilization emissions and soil temperature
 385 (isolines in unit of $^{\circ}\text{C}$) during the case period (October 1st–10th). The sensitivity of Nr emissions to
 386 (c) soil water content (SWC) and (d) soil temperature. (e–j) Daily observed (black line) and
 387 simulated (blue and red bars) NH_3 , HONO, ammonium, nitrate, O_3 and $\text{PM}_{2.5}$ concentration in
 388 Nanjing during the pollution episode.

389 To quantitatively understand the enhanced secondary pollution by soil Nr emissions, we
390 diagnosed the chemical processes in the YRD region. As shown in Figure 5, with fertilization
391 emissions, the average simulated HONO and NH₃ mixing ratio in the YRD region increased by 0.5
392 ppb (118.5%) and 5.9 ppb (39.7%), respectively. The photolysis of HONO is an important source
393 of atmospheric OH that regulates the atmospheric oxidizing capacity and the production of
394 secondary pollutants such as O₃. Along with the enhanced HONO, the OH and O₃ also increased by
395 11.0% (Figure S13b) and 2.5% (Figure 5e), respectively. Diagnostic analysis showed that such
396 enhanced atmospheric oxidizing capacity facilitates the formation of HNO₃ by accelerating the
397 chemical conversion of NO_x to HNO₃ (Figure 5c). Moreover, the soil-emitted NH₃ facilitates the
398 HNO₃ gas-particulate conversion by neutralizing HNO₃ gas, thus facilitating particulate nitrate
399 formation (Figure 5d). The increased emissions of HONO and NH₃ each play a dominant role in the
400 two major steps required for NO₃⁻ production, collectively contributing to the overall production of
401 nitrate (Figure 5g). Thus, sensitivity experiments showed that the joint effects of HONO and
402 NH₃ emissions on nitrate formation are larger than the sum of the individual impacts (Figure S12).
403 Such nonlinear response of the nitrate formation is mainly caused by thermodynamic equilibrium as
404 detailed in Text S2. This single fertilization event resulted in a 18.2% increase in nitrate
405 concentrations in YRD, demonstrating the significance of crop fertilization in Nr emissions and
406 regional air pollution.

407 The responses of nitrate production show great regional disparities depending on its chemical
408 sensitivity to NH₃ or HNO₃ according to the thermodynamic equilibrium principle^{14,73}. For the YRD
409 region, where the nitrate formation regime is mainly NH₃-limited⁷⁴, increasing NH₃ alone
410 significantly enhanced nitrate formation (Figure S16, S17). Besides, the secondary formation of
411 sulfate can also be influenced by NH₃. For instance, the rate of sulfate formation pathways like

412 aqueous-phase oxidation of SO₂ by NO₂, O₃, and Mn-catalyzed oxidation on aerosol surfaces, are
 413 positively correlated to aerosol pH⁷⁵. In NH₃-limited regime, the aerosol pH notably increased with
 414 excess NH₃ due to lower aqueous H⁺ concentrations⁷⁶, likely resulting in a higher sulfate formation
 415 rate during this pollution event.



416
 417 Figure 5. Impacts of soil Nr emissions after fertilization on O₃ and secondary aerosol pollution in
 418 the YRD region. Distribution of enhanced (a) HONO, (b) NH₃, (c) HNO₃ chemical production, (d)
 419 HNO₃ gas-particle conversion, (e) O₃, and (f) nitrate concentration by fertilization Nr emissions
 420 during 1st–10th October 2021. (g) The key processes and factors driving the O₃ and nitrate formation
 421 in the map area.

422 Though fertilization-induced emissions of nitrogen-containing trace gases are dynamically
 423 depicted in this work, some limitations and uncertainties need further efforts. In our simulations, it
 424 is assumed that all fields within a single grid applied fertilizer on the same day, which might not be
 425 that realistic and thus introduce some biases in emission estimation. Furthermore, our simulations

426 only considered fertilizer emissions from drylands, which means the impact of soil emissions on air
427 quality could be even greater while taking other agricultural land types (e.g., rice paddies) into
428 account. Additionally, the rewetting of soils through rainfall or irrigation can trigger nitrogenous
429 gas emissions (the Birch effect)⁷⁷⁻⁷⁹, which was not accounted for in our simulations. Despite these
430 limitations, our results clearly demonstrate the significant influence and spatial heterogeneity of
431 agricultural emissions on air quality and the necessity of including them in air quality modelling.

432

433 **4. IMPLICATIONS**

434 We developed a novel fertilization identification method and a dynamic emission model to access
435 soil Nr emissions and their combined impacts on air pollution in China, with a specific focus on the
436 agriculture-intensive YRD region. Compared to the widely used monthly emission rates based on
437 static statistics, the updated agricultural emission estimation in this work is capable of depicting
438 high-resolution Nr emissions by pinpointing fertilization activities and considering time- and
439 spatial-varying meteorological and soil conditions. When coupling with air quality model, dynamic
440 NH₃ and HONO emissions would more accurately capture the day-to-day variability in the ambient
441 concentration of PM_{2.5} and O₃ precursors. Such dynamic emission and its coupling with air quality
442 model could shed more light on the role of fertilization on regional air quality, particularly during
443 post-fertilization period. Our simulations show that Nr emissions from a typical fertilization event
444 collectively contribute to a 2.5% increase in ozone concentrations and a 18.2% enhancement in
445 nitrate levels over the YRD region. As China's pollutant emissions controls have been relatively
446 stringent for the industrial and transportation sectors in the past decade, the impacts of soil emissions
447 on the nitrogen cycle and atmospheric environment are expected to be increasingly prominent,
448 especially during the fertilization period. Given that there are no specific regulations and standards
449 for controlling emissions of air pollutants from agricultural activities currently, it is of great urgency

450 to investigate the impacts of agricultural emissions on air pollution and to incorporate them into
451 future air quality improvement strategies. Additionally, there is a need for more comprehensive and
452 accurate data regarding agricultural management, such as fertilizer application rate, timing, types
453 and locations of fertilizer uses, which are essential for developing effective models and making
454 informed and cost-effective decisions. By addressing these research gaps, more targeted strategies
455 to mitigate the adverse effects of agriculture on air quality could be achieved.

456 **ASSOCIATED CONTENT**

457 **Supporting Information**

458 Detailed parameterized HONO source mechanisms included in the model; explanation of methods
459 and modeling parameters employed; data quality control and model evaluation with observed air
460 pollutants and meteorological elements; simulated daily average soil water content distribution in
461 Jiangsu; model simulated impacts of soil NH₃, HONO and NO emissions after fertilization in the
462 YRD region.

463 **AUTHOR INFORMATION**

464 **Corresponding Author**

465 Xin Huang – Joint International Research Laboratory of Atmospheric and Earth System Sciences,
466 School of Atmospheric Sciences, Nanjing University, Nanjing 210023, China; Jiangsu Provincial
467 Collaborative Innovation Center for Climate Change, Nanjing 210023, China; ORCID: 0000-0003-
468 0922-5014; Email: xinquang@nju.edu.cn

469 Tao Wang – Department of Civil and Environmental Engineering, Hong Kong Polytechnic
470 University, Hong Kong 99907, China; ORCID: 0000-0002-4765-9377; Phone: +00852-27666059;
471 Email: tao.wang@polyu.edu.hk

472 **Authors**

473 Chuanhua Ren – Department of Civil and Environmental Engineering, Hong Kong Polytechnic
474 University, Hong Kong 99907, China; Joint International Research Laboratory of Atmospheric and
475 Earth System Sciences, School of Atmospheric Sciences, Nanjing University, Nanjing 210023,
476 ORCID: 0000-0002-2606-813X

477 Yanan Wang – Department of Civil and Environmental Engineering, Hong Kong Polytechnic
478 University, Hong Kong 99907, China;

479 Li Zhang – California Air Resources Board, Riverside, CA 92507, USA

480 Xueyu Zhou – Joint International Research Laboratory of Atmospheric and Earth System Sciences,
481 School of Atmospheric Sciences, Nanjing University, Nanjing 210023, China;

482 Weihang Sun – Department of Civil and Environmental Engineering, Hong Kong Polytechnic
483 University, Hong Kong 99907, China;

484 Haoran Zhang – Joint International Research Laboratory of Atmospheric and Earth System Sciences,
485 School of Atmospheric Sciences, Nanjing University, Nanjing 210023, China;

486 Tengyu Liu – Joint International Research Laboratory of Atmospheric and Earth System Sciences,
487 School of Atmospheric Sciences, Nanjing University, Nanjing 210023, China; Jiangsu Provincial
488 Collaborative Innovation Center for Climate Change, Nanjing 210023, China;

489 Aijun Ding – Joint International Research Laboratory of Atmospheric and Earth System Sciences,
490 School of Atmospheric Sciences, Nanjing University, Nanjing 210023, China; Jiangsu Provincial
491 Collaborative Innovation Center for Climate Change, Nanjing 210023, China;

492

493 **Notes**

494 The authors declare no competing financial interest.

495 **Acknowledgment**

496 The authors would like to acknowledge Zhen Wang, Liangyu Wei, and Xingzhao Sun for
497 providing farmers' practices and agricultural management information, and acknowledge Yuliang
498 Liu and Tao Xu for the maintenance of the data instrument. This research was supported by the
499 Hong Kong Research Grants Council (T24–504/17–N), the Ministry of Science and Technology of
500 the People's Republic of China (2022YFC3701105) and the Postgraduate Research & Practice
501 Innovation Program of Jiangsu Province (KYCX24_0204).

502 **Reference**

- 503 (1) Yang, B.; Zhang, T.; Zhang, M.; Li, B. Reactive Nitrogen Releases and Nitrogen Footprint
504 during Intensive Vegetable Production Affected by Partial Human Manure Substitution.
505 *Environ Sci Pollut Res* **2022**, *29* (13), 19572–19582. [https://doi.org/10.1007/s11356-021-](https://doi.org/10.1007/s11356-021-17184-0)
506 [17184-0](https://doi.org/10.1007/s11356-021-17184-0).
- 507 (2) Su, H.; Cheng, Y.; Oswald, R.; Behrendt, T.; Trebs, I.; Meixner, F. X.; Andreae, M. O.; Cheng,
508 P.; Zhang, Y.; Pöschl, U. Soil Nitrite as a Source of Atmospheric HONO and OH Radicals.
509 *Science* **2011**, *333* (6049), 1616–1618. <https://doi.org/10.1126/science.1207687>.
- 510 (3) Lu, X.; Ye, X.; Zhou, M.; Zhao, Y.; Weng, H.; Kong, H.; Li, K.; Gao, M.; Zheng, B.; Lin, J.;
511 Zhou, F.; Zhang, Q.; Wu, D.; Zhang, L.; Zhang, Y. The Underappreciated Role of Agricultural
512 Soil Nitrogen Oxide Emissions in Ozone Pollution Regulation in North China. *Nat Commun*
513 **2021**, *12* (1), 5021. <https://doi.org/10.1038/s41467-021-25147-9>.
- 514 (4) Bhattarai, H. R.; Wanek, W.; Siljanen, H. M. P.; Ronkainen, J. G.; Liimatainen, M.; Hu, Y.;
515 Nykänen, H.; Biasi, C.; Maljanen, M. Denitrification Is the Major Nitrous Acid Production
516 Pathway in Boreal Agricultural Soils. *Commun Earth Environ* **2021**, *2* (1), 1–10.
517 <https://doi.org/10.1038/s43247-021-00125-7>.
- 518 (5) Delon, C.; Galy-Lacaux, C.; Serça, D.; Loubet, B.; Camara, N.; Gardrat, E.; Saneh, I.; Fensholt,
519 R.; Tagesson, T.; Le Dantec, V.; Sambou, B.; Diop, C.; Mougouin, E. Soil and Vegetation-
520 Atmosphere Exchange of NO, NH₃, and N₂O from Field Measurements in a Semi Arid Grazed
521 Ecosystem in Senegal. *Atmospheric Environment* **2017**, *156*, 36–51.
522 <https://doi.org/10.1016/j.atmosenv.2017.02.024>.
- 523 (6) Luo, L.; Cohan, D. S.; Gurung, R. B.; Venterea, R. T.; Ran, L.; Benson, V.; Yuan, Y. Impacts
524 Assessment of Nitrification Inhibitors on U.S. Agricultural Emissions of Reactive Nitrogen
525 Gases. *Journal of Environmental Management* **2024**, *359*, 121043.
526 <https://doi.org/10.1016/j.jenvman.2024.121043>.
- 527 (7) Xue, C.; Ye, C.; Zhang, C.; Catoire, V.; Liu, P.; Gu, R.; Zhang, J.; Ma, Z.; Zhao, X.; Zhang,
528 W.; Ren, Y.; Krysztofiak, G.; Tong, S.; Xue, L.; An, J.; Ge, M.; Mellouki, A.; Mu, Y. Evidence
529 for Strong HONO Emission from Fertilized Agricultural Fields and Its Remarkable Impact on

- 530 Regional O₃ Pollution in the Summer North China Plain. *ACS Earth Space Chem.* **2021**, *5* (2),
531 340–347. <https://doi.org/10.1021/acsearthspacechem.0c00314>.
- 532 (8) Oikawa, P. Y.; Ge, C.; Wang, J.; Eberwein, J. R.; Liang, L. L.; Allsman, L. A.; Grantz, D. A.;
533 Jenerette, G. D. Unusually High Soil Nitrogen Oxide Emissions Influence Air Quality in a
534 High-Temperature Agricultural Region. *Nat Commun* **2015**, *6* (1), 8753.
535 <https://doi.org/10.1038/ncomms9753>.
- 536 (9) Pan, S.-Y.; He, K.-H.; Liao, Y.-L. Fertilization-Induced Reactive Nitrogen Gases and Carbon
537 Dioxide Emissions: Insight to the Carbon-Nitrogen Cycles. *Sustainable Environment Research*
538 **2023**, *33* (1), 23. <https://doi.org/10.1186/s42834-023-00185-8>.
- 539 (10) Xue, C.; Ye, C.; Lu, K.; Liu, P.; Zhang, C.; Su, H.; Bao, F.; Cheng, Y.; Wang, W.; Liu, Y.;
540 Catoire, V.; Ma, Z.; Zhao, X.; Song, Y.; Ma, X.; McGillen, M. R.; Mellouki, A.; Mu, Y.; Zhang,
541 Y. Reducing Soil-Emitted Nitrous Acid as a Feasible Strategy for Tackling Ozone Pollution.
542 *Environ. Sci. Technol.* **2024**, *58* (21), 9227–9235.
- 543 (11) Luo, L.; Ran, L.; Rasool, Q. Z.; Cohan, D. S. Integrated Modeling of U.S. Agricultural Soil
544 Emissions of Reactive Nitrogen and Associated Impacts on Air Pollution, Health, and Climate.
545 *Environ. Sci. Technol.* **2022**, *56* (13), 9265–9276. <https://doi.org/10.1021/acs.est.1c08660>.
- 546 (12) Emmanouil, C.; Drositi, E.; Vasilatou, V.; Diapouli, E.; Krikonis, K.; Eleftheriadis, K.;
547 Kungolos, A. Study on Particulate Matter Air Pollution, Source Origin, and Human Health
548 Risk Based of PM₁₀ Metal Content in Volos City, Greece. *Toxicological & Environmental*
549 *Chemistry* **2017**, *99* (4), 691–709. <https://doi.org/10.1080/02772248.2016.1242005>.
- 550 (13) Oprea, M.; Dunea, D.; Liu, H.-Y. Development of a Knowledge Based System for Analyzing
551 Particulate Matter Air Pollution Effects on Human Health. *Environmental engineering and*
552 *management journal* **2017**, *16*, 669–676. <https://doi.org/10.30638/eemj.2017.068>.
- 553 (14) Seinfeld, J. H.; Pandis, S. N. Atmospheric Chemistry and Physics: From Air Pollution to
554 Climate Change. 2016, 3rd ed. John Wiley, Hoboken, NJ, pp. 412–414.
- 555 (15) Wang, Y.; Zhang, Q. Q.; He, K.; Zhang, Q.; Chai, L. Sulfate-Nitrate-Ammonium Aerosols over
556 China: Response to 2000–2015 Emission Changes of Sulfur Dioxide, Nitrogen Oxides, and
557 Ammonia. *Atmospheric Chemistry and Physics* **2013**, *13* (5), 2635–2652.
558 <https://doi.org/10.5194/acp-13-2635-2013>.
- 559 (16) Liu, M.; Huang, X.; Song, Y.; Tang, J.; Cao, J.; Zhang, X.; Zhang, Q.; Wang, S.; Xu, T.; Kang,
560 L.; Cai, X.; Zhang, H.; Yang, F.; Wang, H.; Yu, J. Z.; Lau, A. K. H.; He, L.; Huang, X.; Duan,
561 L.; Ding, A.; Xue, L.; Gao, J.; Liu, B.; Zhu, T. Ammonia Emission Control in China Would
562 Mitigate Haze Pollution and Nitrogen Deposition, but Worsen Acid Rain. *Proceedings of the*
563 *National Academy of Sciences* **2019**, *116* (16), 7760–7765.
564 <https://doi.org/10.1073/pnas.1814880116>.
- 565 (17) Val Martin, M.; Blanc-Betes, E.; Fung, K. M.; Kantzas, E.; Kantola, I.; Chiaravalloti, I.; Taylor,
566 L.; Emmons, L.; Wieder, W.; Planavsky, N.; Masters, M.; DeLucia, E.; Tai, A.; Beerling, D.
567 Improving Nitrogen Cycling in a Land Surface Model (CLM5) to Quantify Soil N₂O, NO,
568 and NH₃ Emissions from Enhanced Rock Weathering with Croplands. *Geoscientific Model*
569 *Development* **2023**, *16*, 5783–5801. <https://doi.org/10.5194/gmd-16-5783-2023>.

- 570 (18) Fung, K. M.; Val Martin, M.; Tai, A. P. K. Modeling the Interinfluence of Fertilizer-Induced
571 NH₃ Emission, Nitrogen Deposition, and Aerosol Radiative Effects Using Modified CESM2.
572 *Biogeosciences* **2022**, *19* (6), 1635–1655. <https://doi.org/10.5194/bg-19-1635-2022>.
- 573 (19) Li, B.; Chen, L.; Shen, W.; Jin, J.; Wang, T.; Wang, P.; Yang, Y.; Liao, H. Improved Gridded
574 Ammonia Emission Inventory in China. *Atmospheric Chemistry and Physics* **2021**, *21* (20),
575 15883–15900. <https://doi.org/10.5194/acp-21-15883-2021>.
- 576 (20) Pleim, J. E.; Ran, L.; Appel, W.; Shephard, M. W.; Cady-Pereira, K. New Bidirectional
577 Ammonia Flux Model in an Air Quality Model Coupled With an Agricultural Model. *Journal*
578 *of Advances in Modeling Earth Systems* **2019**, *11* (9), 2934–2957.
579 <https://doi.org/10.1029/2019MS001728>.
- 580 (21) Ren, C.; Huang, X.; Liu, T.; Song, Y.; Wen, Z.; Liu, X.; Ding, A.; Zhu, T. A Dynamic
581 Ammonia Emission Model and the Online Coupling with WRF–Chem (WRF–SoilN–Chem
582 v1.0): Development and Regional Evaluation in China. *Geosci. Model Dev.* **2023**, *16* (6), 1641–
583 1659. <https://doi.org/10.5194/gmd-16-1641-2023>.
- 584 (22) Yienger, J. J.; Levy II, H. Empirical Model of Global Soil-Biogenic NO_x Emissions. *Journal*
585 *of Geophysical Research: Atmospheres* **1995**, *100* (D6), 11447–11464.
586 <https://doi.org/10.1029/95JD00370>.
- 587 (23) Guenther, A. B.; Jiang, X.; Heald, C. L.; Sakulyanontvittaya, T.; Duhl, T.; Emmons, L. K.;
588 Wang, X. The Model of Emissions of Gases and Aerosols from Nature Version 2.1
589 (MEGAN2.1): An Extended and Updated Framework for Modeling Biogenic Emissions.
590 *Geoscientific Model Development* **2012**, *5* (6), 1471–1492. <https://doi.org/10.5194/gmd-5-1471-2012>.
- 592 (24) Hudman, R. C.; Moore, N. E.; Mebust, A. K.; Martin, R. V.; Russell, A. R.; Valin, L. C.; Cohen,
593 R. C. Steps towards a Mechanistic Model of Global Soil Nitric Oxide Emissions:
594 Implementation and Space Based-Constraints. *Atmospheric Chemistry and Physics* **2012**, *12*
595 (16), 7779–7795. <https://doi.org/10.5194/acp-12-7779-2012>.
- 596 (25) Sha, T.; Ma, X.; Zhang, H.; Janecek, N.; Wang, Y.; Wang, Y.; Castro García, L.; Jenerette,
597 G. D.; Wang, J. Impacts of Soil NO_x Emission on O₃ Air Quality in Rural California. *Environ.*
598 *Sci. Technol.* **2021**, *55* (10), 7113–7122. <https://doi.org/10.1021/acs.est.0c06834>.
- 599 (26) Wang, Y.; Fu, X.; Wu, D.; Wang, M.; Lu, K.; Mu, Y.; Liu, Z.; Zhang, Y.; Wang, T. Agricultural
600 Fertilization Aggravates Air Pollution by Stimulating Soil Nitrous Acid Emissions at High Soil
601 Moisture. *Environ. Sci. Technol.* **2021**, *55* (21), 14556–14566.
602 <https://doi.org/10.1021/acs.est.1c04134>.
- 603 (27) Wang, Y.; Fu, X.; Wang, T.; Ma, J.; Gao, H.; Wang, X.; Pu, W. Large Contribution of Nitrous
604 Acid to Soil-Emitted Reactive Oxidized Nitrogen and Its Effect on Air Quality. *Environ. Sci.*
605 *Technol.* **2023**, *57* (9), 3516–3526. <https://doi.org/10.1021/acs.est.2c07793>.
- 606 (28) Jin, J.; Wu, R.; Liu, R. Rice Production and Fertilization in China. *Better Crops International*
607 **2002**, *16*, 26–29.
- 608 (29) Sun, X.; Ritzema, H.; Huang, X.; Bai, X.; Hellegers, P. Assessment of Farmers’ Water and
609 Fertilizer Practices and Perceptions in the North China Plain. *Irrigation and Drainage* **2022**,
610 *71* (4), 980–996. <https://doi.org/10.1002/ird.2719>.

- 611 (30) *Crop Calendar Charts*. <https://ipad.fas.usda.gov/ogamaps/cropcalendar.aspx> (accessed 2023-
612 12-12).
- 613 (31) *Survey shows how — and when — farmers use fertilizer*.
614 <https://www.farmprogress.com/crops/survey-shows-how-and-when-farmers-use-fertilizer>
615 (accessed 2024-01-29).
- 616 (32) Crotty, F.; McCalman, H.; Powell, H.; Buckingham, S.; Marley, C. Should Farmers Apply
617 Fertilizer According to When Their Daffodils Are in Flower? Utilizing a “Farmer-Science”
618 Approach to Understanding the Impact of Soil Temperature on Spring N Fertilizer Application
619 in Wales. *Soil Use and Management* **2019**, *35* (1), 169–176. <https://doi.org/10.1111/sum.12503>.
- 620 (33) *Notice of the General Office of the Ministry of Agriculture on issuing the Implementation Plan*
621 *for Promoting the Integration of Water and Fertilizer (2016-2020)*.
622 http://www.moa.gov.cn/nybg/b/2016/diwuqi/201711/t20171127_5920793.htm (accessed
623 2024-06-21).
- 624 (34) *Integration of water and fertilizer in China Agricultural Technical Services Manual*.
625 <http://www.jsogg.com.cn/Files/PictureDocument/20170216122923179831343060.pdf>
626 (accessed 2024-06-21).
- 627 (35) Follmer, C. M.; Hummes, A. P.; Lângaro, N. C.; Petry, C.; Moterle, D. F.; Bortoluzzi, E. C.
628 Nutrient Availability and pH Level Affect Germination Traits and Seedling Development of
629 *Conyza Canadensis*. *Sci Rep* **2021**, *11* (1), 15607. [https://doi.org/10.1038/s41598-021-95164-
630 **7**.](https://doi.org/10.1038/s41598-021-95164-7)
- 631 (36) Liao, Q.; Nie, J.; Yin, H.; Luo, Y.; Shu, C.; Cheng, Q.; Fu, H.; Li, B.; Li, L.; Sun, Y.; Chen, Z.;
632 Ma, J.; Li, N.; Zhang, X.; Yang, Z. Can the Integration of Water and Fertilizer Promote the
633 Sustainable Development of Rice Production in China? *Agriculture* **2024**, *14* (4), 585.
634 <https://doi.org/10.3390/agriculture14040585>.
- 635 (37) ADEOS-II AMSR Soil Moisture Algorithm.
636 https://www.eorc.jaxa.jp/AMSR/satellite/pdf.adeos-ii/alg_des.pdf (accessed 2024-06-21).
- 637 (38) Reichle, R. H.; Jackson, T.; Kimball, J.; Koster, R. D. Soil Moisture Active Passive (SMAP)
638 Project Assessment Report for the Beta-Release L4_SM Data Product.
- 639 (39) Draper, C. S.; Walker, J. P.; Steinle, P. J.; de Jeu, R. A. M.; Holmes, T. R. H. An Evaluation of
640 AMSR–E Derived Soil Moisture over Australia. *Remote Sensing of Environment* **2009**, *113* (4),
641 703–710. <https://doi.org/10.1016/j.rse.2008.11.011>.
- 642 (40) Lal, P.; Singh, G.; Das, N. N.; Colliander, A.; Entekhabi, D. Assessment of ERA5-Land
643 Volumetric Soil Water Layer Product Using In Situ and SMAP Soil Moisture Observations.
644 *IEEE Geoscience and Remote Sensing Letters* **2022**, *19*, 1–5.
645 <https://doi.org/10.1109/LGRS.2022.3223985>.
- 646 (41) Martens, B.; Miralles, D. G.; Lievens, H.; van der Schalie, R.; de Jeu, R. A. M.; Fernández-
647 Prieto, D.; Beck, H. E.; Dorigo, W. A.; Verhoest, N. E. C. GLEAM v3: Satellite-Based Land
648 Evaporation and Root-Zone Soil Moisture. *Geosci. Model Dev.* **2017**, *10* (5), 1903–1925.
649 <https://doi.org/10.5194/gmd-10-1903-2017>.
- 650 (42) Sakai, T.; Iizumi, T.; Okada, M.; Nishimori, M.; Grünwald, T.; Prueger, J.; Cescatti, A.; Korres,
651 W.; Schmidt, M.; Carrara, A.; Loubet, B.; Ceschia, E. Varying Applicability of Four Different

- 652 Satellite-Derived Soil Moisture Products to Global Gridded Crop Model Evaluation.
653 *International Journal of Applied Earth Observation and Geoinformation* **2016**, *48*, 51–60.
654 <https://doi.org/10.1016/j.jag.2015.09.011>.
- 655 (43) *The third national land resource survey*. [http://agri.china.com.cn/2021-](http://agri.china.com.cn/2021-08/27/content_41656841.htm)
656 [08/27/content_41656841.htm](http://agri.china.com.cn/2021-08/27/content_41656841.htm) (accessed 2024-02-11).
- 657 (44) Wang, J.; Ma, W.; Jiang, R.; Zhang, F. Analysis about Amount and Ratio of Basal Fertilizer
658 and Topdressing Fertilizer on Rice, Wheat, Maize in China. *Chinese Journal of Soil Science*.
659 **2008**, *39* (2), 329-333.
- 660 (45) Oswald, R.; Behrendt, T.; Ermel, M.; Wu, D.; Su, H.; Cheng, Y.; Breuninger, C.; Moravek, A.;
661 Mougou, E.; Delon, C.; Loubet, B.; Pommerening-Röser, A.; Sörgel, M.; Pöschl, U.; Hoffmann,
662 T.; Andreae, M. O.; Meixner, F. X.; Trebs, I. HONO Emissions from Soil Bacteria as a Major
663 Source of Atmospheric Reactive Nitrogen. *Science* **2013**, *341* (6151), 1233–1235.
664 <https://doi.org/10.1126/science.1242266>.
- 665 (46) Zhang, L.; Wang, T.; Zhang, Q.; Zheng, J.; Xu, Z.; Lv, M. Potential Sources of Nitrous Acid
666 (HONO) and Their Impacts on Ozone: A WRF-Chem Study in a Polluted Subtropical Region:
667 MODELING HONO IN A SUBTROPICAL REGION. *J. Geophys. Res. Atmos.* **2016**, *121* (7),
668 3645–3662. <https://doi.org/10.1002/2015JD024468>.
- 669 (47) Li, M.; Liu, H.; Geng, G.; Hong, C.; Liu, F.; Song, Y.; Tong, D.; Zheng, B.; Cui, H.; Man, H.;
670 Zhang, Q.; He, K. Anthropogenic Emission Inventories in China: A Review. *National Science*
671 *Review* **2017**, *4* (6), 834–866. <https://doi.org/10.1093/nsr/nwx150>.
- 672 (48) *MEICModel – Tracking Anthropogenic Emissions in China*. <http://meicmodel.org.cn/#firstPage>
673 (accessed 2023-12-12).
- 674 (49) Zhang, Z.; Dong, L.; Liu, P.; Zhou, T., Sun, L.; Nitrogen Flow Characteristics of Agricultural
675 Production and Consumption System in the Yangtze River Delta Region and Its Driving
676 Factors. *Environmental Science* **2024**, *45*(9): 5451-5463.
- 677 (50) Lee, J. A.; Jiménez, P. A.; Kumar, R.; He, C. Impact of Direct Insertion of SMAP Soil Moisture
678 Retrievals in WRF-Chem for Dust Storm Events in the Western U.S. *Atmospheric Environment*
679 **2024**, *321*, 120349. <https://doi.org/10.1016/j.atmosenv.2024.120349>.
- 680 (51) Stein, A. F.; Draxler, R. R.; Rolph, G. D.; Stunder, B. J. B.; Cohen, M. D.; Ngan, F. NOAA’s
681 HYSPLIT Atmospheric Transport and Dispersion Modeling System. *Bulletin of the American*
682 *Meteorological Society* **2015**, *96* (12), 2059–2077. [https://doi.org/10.1175/BAMS-D-14-](https://doi.org/10.1175/BAMS-D-14-00110.1)
683 [00110.1](https://doi.org/10.1175/BAMS-D-14-00110.1).
- 684 (52) Liu, R.; Liu, T.; Huang, X.; Ren, C.; Wang, L.; Niu, G.; Yu, C.; Zhang, Y.; Wang, J.; Qi, X.;
685 Nie, W.; Chi, X.; Ding, A. Characteristics and Sources of Atmospheric Ammonia at the
686 SORPES Station in the Western Yangtze River Delta of China. *Atmospheric Environment* **2024**,
687 *318*, 120234. <https://doi.org/10.1016/j.atmosenv.2023.120234>.
- 688 (53) Liu, Y.; Nie, W.; Xu, Z.; Wang, T.; Wang, R.; Li, Y.; Wang, L.; Chi, X.; Ding, A. Semi-
689 Quantitative Understanding of Source Contribution to Nitrous Acid (HONO) Based on 1 Year
690 of Continuous Observation at the SORPES Station in Eastern China. *Atmospheric Chemistry*
691 *and Physics* **2019**, *19* (20), 13289–13308. <https://doi.org/10.5194/acp-19-13289-2019>.

- 692 (54) *China National Environmental Monitoring Centre Homepage*. <https://www.cnemc.cn/>
693 (accessed 2024-06-29).
- 694 (55) Mladenova, I.; Lakshmi, V.; Jackson, T. J.; Walker, J. P.; Merlin, O.; de Jeu, R. A. M.
695 Validation of AMSR-E Soil Moisture Using L-Band Airborne Radiometer Data from National
696 Airborne Field Experiment 2006. *Remote Sensing of Environment* **2011**, *115* (8), 2096–2103.
697 <https://doi.org/10.1016/j.rse.2011.04.011>.
- 698 (56) Hersbach, H.; Bell, B.; Berrisford, P.; Hirahara, S.; Horányi, A.; Muñoz-Sabater, J.; Nicolas,
699 J.; Peubey, C.; Radu, R.; Schepers, D.; Simmons, A.; Soci, C.; Abdalla, S.; Abellan, X.;
700 Balsamo, G.; Bechtold, P.; Biavati, G.; Bidlot, J.; Bonavita, M.; De Chiara, G.; Dahlgren, P.;
701 Dee, D.; Diamantakis, M.; Dragani, R.; Flemming, J.; Forbes, R.; Fuentes, M.; Geer, A.;
702 Haimberger, L.; Healy, S.; Hogan, R. J.; Hólm, E.; Janisková, M.; Keeley, S.; Laloyaux, P.;
703 Lopez, P.; Lupu, C.; Radnoti, G.; de Rosnay, P.; Rozum, I.; Vamborg, F.; Villaume, S.; Thépaut,
704 J.-N. The ERA5 Global Reanalysis. *Quarterly Journal of the Royal Meteorological Society*
705 **2020**, *146* (730), 1999–2049. <https://doi.org/10.1002/qj.3803>.
- 706 (57) Dong, X.; Lai, X.; Wang, Y.; Dong, W.; Zhu, J.; Dong, L.; Cen, S. Applicability Evaluation of
707 Multiple Sets of Soil Moisture Data on the Tibetan Plateau. *Frontiers in Earth Science* **2022**,
708 *10*, 1–18.
- 709 (58) Jägermeyr, J.; Müller, C.; Minoli, S.; Ray, D.; Siebert, S. GGCM Phase 3 Crop Calendar, 2021.
710 <https://doi.org/10.5281/zenodo.5062513>.
- 711 (59) Huo, K.; Ruan, Y.; Fan, H.; Guo, C.; Cai, H. Spatial-Temporal Variation Characteristics of
712 Cultivated Land and Controlling Factors in the Yangtze River Delta Region of China. *Frontiers*
713 *in Environmental Science* **2022**, *10*, 1–18.
- 714 (60) Qiu, B.; Hu, X.; Chen, C.; Tang, Z.; Yang, P.; Zhu, X.; Yan, C.; Jian, Z. Maps of Cropping
715 Patterns in China during 2015–2021. *Sci Data* **2022**, *9* (1), 479. <https://doi.org/10.1038/s41597-022-01589-8>.
- 716 (61) Yu, X.; Shen, L.; Hou, X.; Yuan, L.; Pan, Y.; An, J.; Yan, S. High-Resolution Anthropogenic
717 Ammonia Emission Inventory for the Yangtze River Delta, China. *Chemosphere* **2020**, *251*,
718 126342. <https://doi.org/10.1016/j.chemosphere.2020.126342>.
- 719 (62) Zang, Y.; Qiu, Y.; Chen, X.; Chen, J.; Yang, W.; Liu, Y.; Peng, L.; Shen, M.; Cao, X. Mapping
720 Rapeseed in China during 2017–2021 Using Sentinel Data: An Automated Approach
721 Integrating Rule-Based Sample Generation and a One-Class Classifier (RSG-OC). *GIScience*
722 *& Remote Sensing* **2023**, *60* (1), 2163576. <https://doi.org/10.1080/15481603.2022.2163576>.
- 723 (63) Xu, W.; Zhang, L.; Liu, X. A Database of Atmospheric Nitrogen Concentration and Deposition
724 from the Nationwide Monitoring Network in China. *Sci Data* **2019**, *6* (1), 51.
725 <https://doi.org/10.1038/s41597-019-0061-2>.
- 726 (64) Xia, W., Zhou, W., Liang, G., Wang, X., Sun, J., Li, S. Study on ammonia volatilization loss
727 from nitrogen fertilizer in the rice-wheat rotation system under optimized nitrogen application.
728 *Journal of Plant Nutrition and Fertilizers* **2010**, *16*(1), 6–13.
- 729 (65) Liu, L., Cao, Y., Tian, Y., Yin, B., Zhu, Z. Study on soil ammonia volatilization and nitric
730 oxide emissions during the winter wheat season in the Taihu region. *Journal of Plant Nutrition*
731 *and Fertilizers* **2013**, *19*(6), 1420–1427.
- 732

- 733 (66) Crop sowing guideline, *the Ministry of Agriculture and Rural Affairs*.
734 <http://zdscxx.moa.gov.cn:8080/nyb/pc/calendar.jsp> (accessed 2023-12-20).
- 735 (67) Evangeliou, N.; Balkanski, Y.; Eckhardt, S.; Cozic, A.; Van Damme, M.; Coheur, P.-F.;
736 Clarisse, L.; Shephard, M. W.; Cady-Pereira, K. E.; Hauglustaine, D. 10-Year Satellite-
737 Constrained Fluxes of Ammonia Improve Performance of Chemistry Transport Models.
738 *Atmospheric Chemistry and Physics* **2021**, *21* (6), 4431–4451. [https://doi.org/10.5194/acp-21-](https://doi.org/10.5194/acp-21-4431-2021)
739 [4431-2021](https://doi.org/10.5194/acp-21-4431-2021).
- 740 (68) Liu, P.; Xue, C.; Ye, C.; Liu, C.; Zhang, C.; Wang, J.; Zhang, Y.; Liu, J.; Mu, Y. The Lack of
741 HONO Measurement May Affect the Accurate Diagnosis of Ozone Production Sensitivity.
742 *ACS Environ. Au* **2023**, *3* (1), 18–23.
- 743 (69) Zhao, M., Tian, Y., Zhang, M., Yao, Y., Yin, B., Zhu, Z. Reducing NH₃ and NO emissions
744 from rice-wheat rotation in the Taihu region through improved agronomic management
745 practices. *Soil* **2015**, *47*(5), 836–841.
- 746 (70) Ali, M.; Haruna, A. O.; Majid, N. M. A.; Primus, W. C.; Maikol, N.; Asap, A.; Naharuddin, A.
747 N.; Jeffary, A. V. Using Soil Water to Control Ammonia Emission from Acid Soils with and
748 Without Chicken Litter Biochar. *SAR* **2019**, *8* (3), 23. <https://doi.org/10.5539/sar.v8n3p23>.
- 749 (71) Farquhar, G. D.; Firth, P. M.; Wetselaar, R.; Weir, B. On the Gaseous Exchange of Ammonia
750 between Leaves and the Environment: Determination of the Ammonia Compensation Point.
751 **1980**, *66*(4), 710–714.
- 752 (72) Baobin H.; Peng C.; Yihang Y. The characteristics of soil HONO emission and emission factors
753 after fertilization. *Acta Scientiae Circumstantiae* **2021**, *42*(8), 449–458
- 754 (73) Determining_limiting_and_excess_reagents_1.Pdf.
755 [https://www.uah.edu/images/administrative/student-success-](https://www.uah.edu/images/administrative/student-success-center/resources/handouts/handouts_2019/determining_limiting_and_excess_reagents_1.pdf)
756 [center/resources/handouts/handouts_2019/determining_limiting_and_excess_reagents_1.pdf](https://www.uah.edu/images/administrative/student-success-center/resources/handouts/handouts_2019/determining_limiting_and_excess_reagents_1.pdf)
757 (accessed 2024-06-23).
- 758 (74) Zhao, Y.; Yuan, M.; Huang, X.; Chen, F.; Zhang, J. Quantification and Evaluation of
759 Atmospheric Ammonia Emissions with Different Methods: A Case Study for the Yangtze
760 River Delta Region, China. *Atmospheric Chemistry and Physics* **2020**, *20* (7), 4275–4294.
761 <https://doi.org/10.5194/acp-20-4275-2020>.
- 762 (75) Wang, T.; Liu, M.; Liu, M.; Song, Y.; Xu, Z.; Shang, F.; Huang, X.; Liao, W.; Wang, W.; Ge,
763 M.; Cao, J.; Hu, J.; Tang, G.; Pan, Y.; Hu, M.; Zhu, T. Sulfate Formation Apportionment during
764 Winter Haze Events in North China. *Environ. Sci. Technol.* **2022**, *56* (12), 7771–7778.
765 <https://doi.org/10.1021/acs.est.2c02533>.
- 766 (76) Liu, M.; Song, Y.; Zhou, T.; Xu, Z.; Yan, C.; Zheng, M.; Wu, Z.; Hu, M.; Wu, Y.; Zhu, T. Fine
767 Particle pH during Severe Haze Episodes in Northern China. *Geophysical Research Letters*
768 **2017**, *44* (10), 5213–5221. <https://doi.org/10.1002/2017GL073210>.
- 769 (77) Mumford, M. T.; Rowlings, D. W.; Scheer, C.; De Rosa, D.; Grace, P. R. Effect of Irrigation
770 Scheduling on Nitrous Oxide Emissions in Intensively Managed Pastures. *Agriculture,*
771 *Ecosystems & Environment* **2019**, *272*, 126–134. <https://doi.org/10.1016/j.agee.2018.11.011>.
- 772 (78) Guo, X.; Drury, C. F.; Yang, X.; Daniel Reynolds, W.; Fan, R. The Extent of Soil Drying and
773 Rewetting Affects Nitrous Oxide Emissions, Denitrification, and Nitrogen Mineralization. *Soil*

774 *Science Society of America Journal* **2014**, 78 (1), 194–204.
775 <https://doi.org/10.2136/sssaj2013.06.0219>.

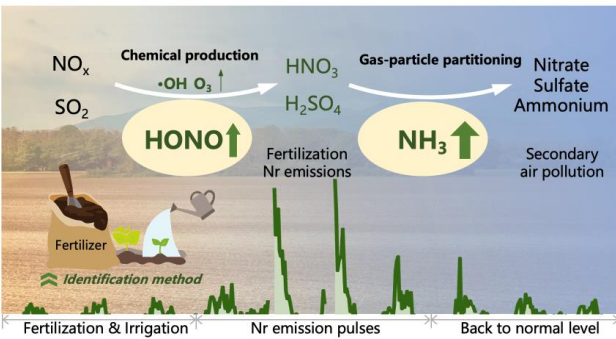
776 (79) Fierer, N.; Schimel, J. P. Effects of Drying–Rewetting Frequency on Soil Carbon and Nitrogen
777 Transformations. *Soil Biology and Biochemistry* **2002**, 34 (6), 777–787.
778 [https://doi.org/10.1016/S0038-0717\(02\)00007-X](https://doi.org/10.1016/S0038-0717(02)00007-X).

779

780

781

782 **For Table of Contents Only**



783